UNCLASSIFIED

SECURITY CLASSIFICATION OF THIS PAGE

JJ 24

REPORT DOCUMENTATION PAGE

1a. REPORT SECURITY CLASSIFICATION UNCLASSIFIED	1b. RESTRICTIVE MARKINGS DTIC FILE COPY
AD-A211 613 ULE BER(S)	3. DISTRIBUTION / AVAILABILITY OF REPORT Approved for public release; distribution is unlimited (2)
	5. MONITORING ORGANIZATION REPORT NUMBER(S) AFOSR-TR- 89-1060
6a. NAME OF PERFORMING ORGANIZATION Stanford University	6b. OFFICE SYMBOL (If applicable)
6c. ADDRESS (City, State, and ZIP Code) Stanford, CA 94305	7a. NAME OF MONITORING ORGANIZATION AFOSR/NC
	7b. ADDRESS (City, State, and ZIP Code) Building 410, Bolling AFB DC 20332-6448
8a. NAME OF FUNDING / SPONSORING ORGANIZATION AFOSR	8b. OFFICE SYMBOL (If applicable) NC
	9. PROCUREMENT INSTRUMENT IDENTIFICATION NUMBER AFOSR-F49620-86-C-0016
8c. ADDRESS (City, State, and ZIP Code) Building 410, Bolling AFB DC 20332-6448	10. SOURCE OF FUNDING NUMBERS

PROGRAM ELEMENT NO.	PROJECT NO.	TASK NO.	WORK UNIT ACCESSION NO.
61102F	2303	B1	

11. TITLE (Include Security Classification)

State-Resolved Reaction Dynamics

12. PERSONAL AUTHOR(S)
Richard N. Zare

13a. TYPE OF REPORT	13b. TIME COVERED	14. DATE OF REPORT (Year, Month, Day)	15. PAGE COUNT
Final	FROM 11/01/85 TO 10/31/88	07/12/89	23

16. SUPPLEMENTARY NOTATION

17. COSATI CODES			18. SUBJECT TERMS (Continue on reverse if necessary and identify by block number)
FIELD	GROUP	SUB-GROUP	

19. ABSTRACT (Continue on reverse if necessary and identify by block number)

See Back

20. DISTRIBUTION / AVAILABILITY OF ABSTRACT	21. ABSTRACT SECURITY CLASSIFICATION
☐ UNCLASSIFIED/UNLIMITED ☐ SAME AS RPT ☐ DTIC USERS	UNCLASSIFIED

22a. NAME OF RESPONSIBLE INDIVIDUAL	22b. TELEPHONE (Include Area Code)	22c. OFFICE SYMBOL
L P DAVIS, LTCOL, USAF	202/767-4963	AFOSR/NC

DD FORM 1473, 84 MAR — 83 APR edition may be used until exhausted. All other editions are obsolete.

SECURITY CLASSIFICATION OF THIS PAGE
UNCLASSIFIED

89 8 10 062

Status of the research effort we have pursued three separate experiments, all of which have had as their focus the understanding of basic processes involving charged species. The significant accomplishments of these experiments and their progress toward achieving the research objective is discussed below:

A. Resonance-Enhanced Multiphoton Ionization-Photoelectron Spectroscopy, (REMPI-PES) of NO

We have designed and contracted a single time-of-flight (TOF) photo-electron spectrometer to be used in conjunction with the MPI of jet-cooled molecules. With this apparatus we have been able to measure energy and single-resolved photoelectron spectra. Such information has been of direct used in measuring the internal state distribution of REMPI-formed ions used in ion-molecule reaction studies. We have also been involvd in the study of the dynamics of the multiphoton ionization process itself.

B. REMPI Spectroscopy of HBr and DBr

The laser-induced fluorescence (LIF) technique has been developed to probe ion species. First, the ions produced directly from REMPI can have their rotational state distribution measured in order to investigate the rotational propensity roles in photoionization processes. Second, the ions produced from a reaction between the state-selected ions generated by REMPI and other molecules can be observed for studying state-to-state ion-molecule reaction dynamics.

C. State-Selected Ion-Molecule Reactions

First, we have studied the reactions of ammonia cations with neutral molecules. These studies were conducted using a tandem quadropole mass spectrometer. We have also completed and created a new tapole ion trap. This instrument was proposed to increase vastly our control over and understanding of biomolecular ion-molecular reactions. To make the quadropole/octapole/quadropole ion trap operational it was necessary to solve the technically challenging problem of interfacing three dissimilar radio frequency (rf) devices. The resulting instrument has extended capabilities, including the measurement of absolute ion-molecule cross sections.

OBJECTIVE OF THE RESEARCH

This research program was directed toward the understanding of basic processes involving charged species. The objective of the research was to investigate the detailed quantum specification of reagents and products in both ion unimolecular dissociation and ion-molecule bimolecular reactions by means of a laser technique that allows state selection of the reagents. We placed emphasis on ion-molecule bimolecular reactions in which laser multiphoton ionization was used in conjunction with photoelectron spectroscopy to prepare ions in a known vibrational state. Once the ions were prepared in a state-selected manner, various ion collision processes were to be studied as a function of both internal and collision energy.

STATUS OF THE RESEARCH EFFORT

Support by this grant has allowed us to pursue three separate experiments, all of which have had as their focus the research objective outlined above. The significant accomplishments of these experiments and their progress toward achieving the research objective is discussed below:

A. Resonance-Enhanced Multiphoton Ionization-Photoelectron Spectroscopy (REMPI-PES) of NO

We have designed and constructed a simple time-of-flight (TOF) photoelectron spectrometer to be used in conjunction with the MPI of jet-cooled

molecules. With this apparatus we have been able to measure energy- and angle-resolved photoelectron spectra. Such information has been of direct used in measuring the internal state distribution of REMPI-formed ions used in ion-molecule reaction studies. We have also been involved in the study of the dynamics of the multiphoton ionization process itself.

Recent modifications of our TOF photoelectron spectrometer have made possible the measurement of rotational state distributions of ions formed by REMPI. A two-color high-resolution energy- and angle-resolved study of the photoelectrons produced in the $(1 + 1')$ REMPI of nitric oxide (NO) via rotational levels of the $A\ ^2\Sigma^+\ v = 0$ state has been completed.[1] Markedly different photoelectron angular distributions arising from production of ions in different rotational states ($\Delta N = -2, -1, 0, +1, +2$ transitions in the ionization step) have been observed (Fig. 1). The $\Delta N = +2$ and -2 angular distributions have been shown to be very sensitive to the intermediate state alignment.

The REMPI process can be described as coupling of ionization continuum channels to the Rydberg orbital of the intermediate state through the dipole operator. These continuum channels are described by the following parameters: photoelectron momentum, k; angular momentum, l; projection of angular momentum on the internuclear axis, λ; and spin projection, m_s. In addition, each scattering channel will have a unique phase shift, $\eta_{l\lambda}$, that will be dictated by the dynamics of the scattering process. In the NO paper, a model has been advanced in which experimental observables (angle- and energy-resolved photoelectron spectra) are used to determine the attributes (relative amplitudes and phase shifts) of a small number of these interfering continuum channels that contribute to the ionization step as well as the fraction of parallel character of the ionization step. In the case of the NO

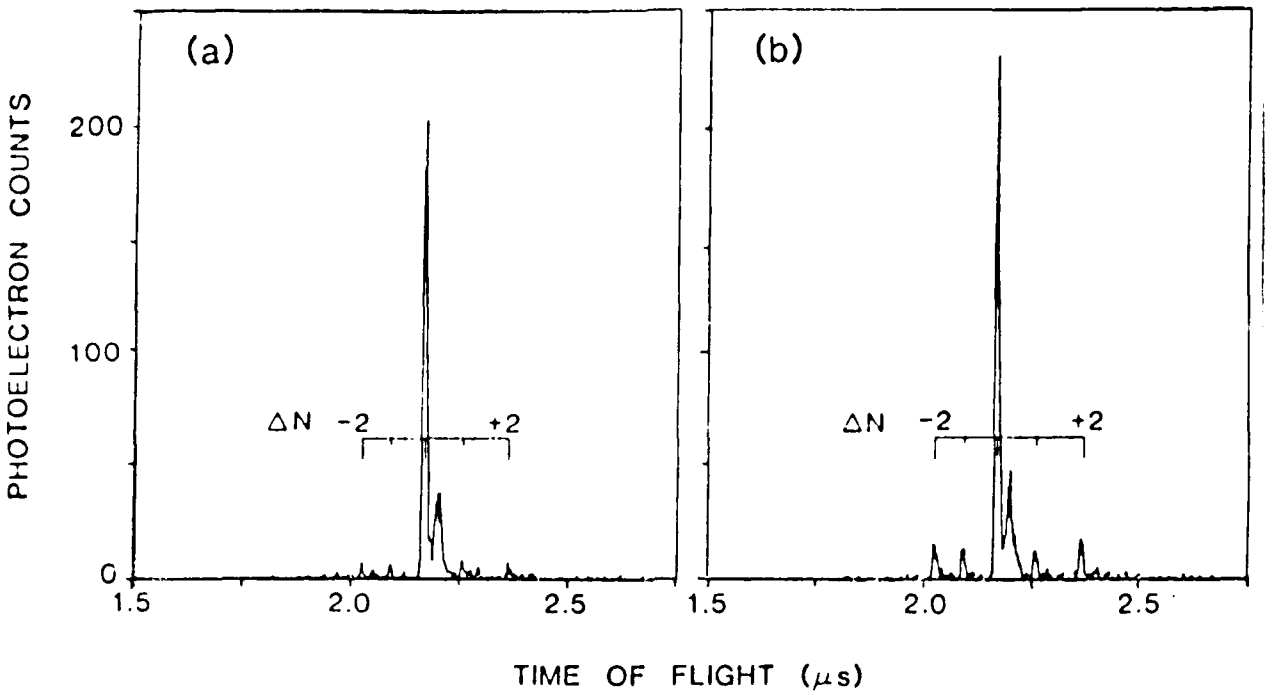

Figure 1. Two-color TOF photoelectron spectra via the NO A-X $Q_{11}+P_{21}(25.5)$ resonant excitation. The electric field vector of the resonant laser is (a) parallel or (b) perpendicular to the detection axis. In both cases the electric field vector of the ionization laser is parallel to the detection axis. Each peak is labeled with ΔN, the change in rotational angular momentum in the ionization transition.

study, nearly 70% of the ejected photoelectrons came from the $\Delta N = 0$ ionization transition; the partial wave composition of these electrons was dominated by p-character ($l = 1$). The smaller $\Delta N = +1$ and -1 peaks had both s- and d-wave character ($l = 0$ and 2, respectively). The $\Delta N = +2$ and -2 photoelectron peaks exhibited far more f-wave ($l = 3$) than p-wave character because destructive interference nearly removed the p-wave contribution to the angular distribution. The partial wave decomposition was used to predict angular distributions resulting from excitation of the intermediate state by different rotational branch transitions; these predictions were shown to be in excellent agreement with the measured distributions.

This model permitted a more quantitative comparison of photoelectron spectra to *ab initio* calculations of the REMPI process than was possible

before our work. Rudolph and McKoy performed such a calculation of the two-color process used in our NO study. The agreement between their results and ours proved to be quite good.

B. REMPI Spectroscopy of HBr and DBr

The laser-induced fluorescence (LIF) technique has been developed to probe ion species. First, the ions produced directly from REMPI can have their rotational state distribution measured in order to investigate the rotational propensity rules in photoionization processes. Second, the ions produced from a reaction between the state-selected ions generated by REMPI and other molecules can be observed for studying state-to-state ion-molecule reaction dynamics.

In our experiment we have measured the (2 + 1) REMPI spectra of HBr and DBr over the range 246–270 nm. The experiment is performed under bulb conditions with the sample gas flowing through the chamber at a pressure of 10–50 mTorr. We can conduct the experiment under collisionless or single-collision conditions by adjusting the delay (10–100 ns) between the REMPI laser and the LIF laser. The REMPI laser is focused down in order to generate a significant ion yield. The lower power ($\sim$ 50 μJ) probe laser beam is unfocused (5 mm diameter) in order to prevent saturation and allow complete probing of all the ions.

Several Rydberg states are found to have strong transitions with well-resolved rotational lines in the HBr and DBr spectra. Since HBr^+ has a ground state configuration $^2\Pi_{1/2,3/2}$ with the splitting about 2600 cm^{-1} between the two spin-orbit components, the Rydberg state of HBr should consist of either a $^2\Pi_{1/2}$ or $^2\Pi_{3/2}$ ion core and a Rydberg electron in Hund's

case (c) coupling scheme. Therefore, spin-orbit component state selection in HBr^+ is expected when it is ionized from its Rydberg states. Additionally, Franck-Condon factors allow only $\Delta v = 0$ transitions between the Rydberg state and the ion due to their similar potentials. We have confirmed this state selection with the photoelectron spectrum of HBr and the LIF spectrum of HBr^+. The $F\ ^1\Delta_2$, $D\ ^1\Pi_1$, $E\ 0^+$, and $f\ ^3\Delta_2$ $v = 0, 1$ states give ion vibrational state and spin-orbit component state selection of 99%, 97%, 90%, and 99%, respectively.

The nascent rotational population of HBr^+ produced from the (2 + 1) REMPI via HBr Rydberg states has been measured by LIF spectroscopy of the HBr^+ $A\ ^2\Sigma - X\ ^2\Pi$ transition. It has shown the rotational levels of HBr^+ to be highly selected. From the nascent distribution of HBr^+ rotational levels, we can conclude the following propensity rules in the ionization transition process: (1) the distribution of HBr^+ $X\ ^2\Pi_{1/2}$ formed from the ionization of Rydberg state $F\ (^2\Pi_{1/2})5p\pi$ shows the selection rule of $+ \longleftrightarrow +, - \longleftrightarrow -$ with $\Delta J = \pm 1/2, \pm 3/2, \pm 5/2$ and $+ \longleftrightarrow -$ and $- \longleftrightarrow +$ with $\Delta J = \pm 1/2, +3/2$. The $+ \longleftrightarrow -$ transitions predominate; (2) the distribution of HBr^+ $X^2\Pi_{3/2}$ formed from the ionization of Rydberg states $f\ ^3\Delta_2$ and $E\ 0^+$ follow rules similar to (1); and (3) the distribution of $X\ ^2\Pi_{1/2}$ formed from the ionization of the $E\ 0^+$ Rydberg state shows only $+ \longleftrightarrow -$ transition, with $\Delta J = +1/2, +3/2$. We have derived the parity selection rule for Hund's case (c); it indicates that the transition with $+ \longleftrightarrow -$ corresponds to only s-wave electron ejection.

C. State-Selected Ion-Molecule Reactions

This section is divided into two parts. In the first, we summarize our

studies of the $NH_3^+(v_2) + CH_3$, $NH_3^+(v_2) + ND_3$ and $ND_3^+(v_2) + NH_3$ systems. These studies were conducted using a tandem quadrupole mass spectrometer. In the second, we describe the newly completed and operational octapole ion trap. This instrument was proposed to increase vastly our control over and understanding of bimolecular ion-molecular reactions such as those above. To make the quadrupole/octapole/quadrupole ion trap operational it was necessary to solve the technically challenging problem of interfacing three dissimilar radio frequency (rf) devices. The resulting instrument has extended capabilities, including the measurement of absolute ion-molecule cross sections.

1. State-selected chemistry of the ammonia ion

Ammonia is an excellent candidate for vibrational state selection by REMPI through its $\tilde{B}$ and $\tilde{C}'$ electronic states. The ground state geometry of the neutral is pyramidal while the two excited Rydberg states and the ground state of the ion have planar equilibrium configurations. The ν_2 umbrella-bending mode is the vibrational motion that connects the pyramidal geometry of the ground state with the planar geometry of the Rydberg states. The result is that the (2+1) MPI spectrum of ammonia in the ultraviolet (280–320 nm) region shown in Fig. 2 consists of two long, interleaves progressions in the ν_2 mode in the $\tilde{B}$ and $\tilde{C}'$ states. Since the geometry changes little in going for the resonant intermediate state to the ground ionic state, the Franck-Condon factors will show the greatest overlap for the $\Delta v = 0$ vibrational state-retaining transition. Resonant MPI via these high-lying Rydberg states is therefore expected to produce predominantly a single vibrational state in the ion. The vibrational level produced corresponds directly to the resonant vibrational level accessed in the Rydberg state.

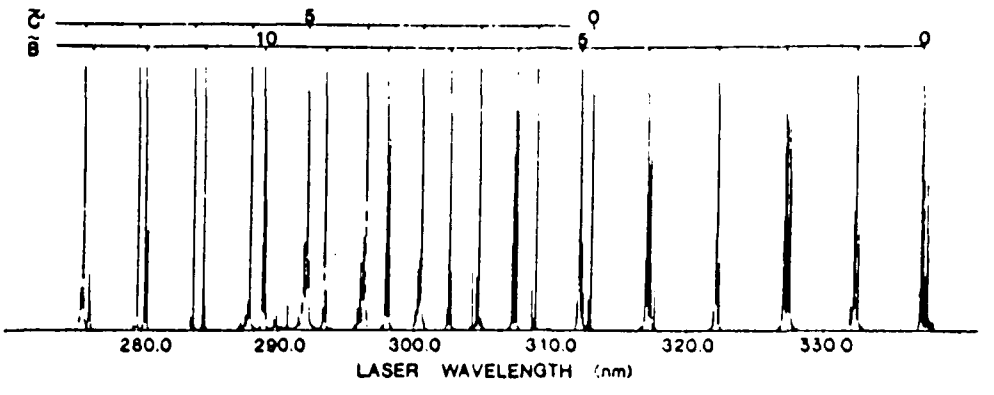

Figure 2. Multiphoton ionization spectrum of ammonia in the region 285–325 nm.

The efficiency of this preparation method is confirmed by analysis of the kinetic energy distribution of the photoelectrons produced in the ionization. This information directly indicates in which vibrational state(s) the ions have been formed. We find that about 90% of the NH_3^+ formed can be prepared in a single vibrational level of the ν_2 umbrella-bending mode (see Fig. 3).

Note the dominant peak in each spectrum corresponding to the state-selected $\Delta v = 0$ vibrational level. The relative populations derived from these spectra demonstrate that the $NH_3^+(\tilde{X},v)$ state can be prepared very efficiently by simply selecting the laser wavelength to be resonant with different vibrational levels in either the $\tilde{B}$ or $\tilde{C}'$ states of the neutral.

The state-selected ion-molecule reaction apparatus (Fig. 4) used for these studies employs a longitudinal beam-gas geometry for investigating the dynamics of ion-molecule reactions. Schematic diagram of the tandem quadrupole mass spectrometer with laser multiphoton ionization source. The frequency-doubled output of a Nd:YAG pumped dye laser is used to ionize a supersonic expansion of ammonia in argon. The NH_3^+ ions are collected by a series of ion optics and focused into a scattering cell containing the neutral target gas. The kinetic energy of the impinging ion beam can

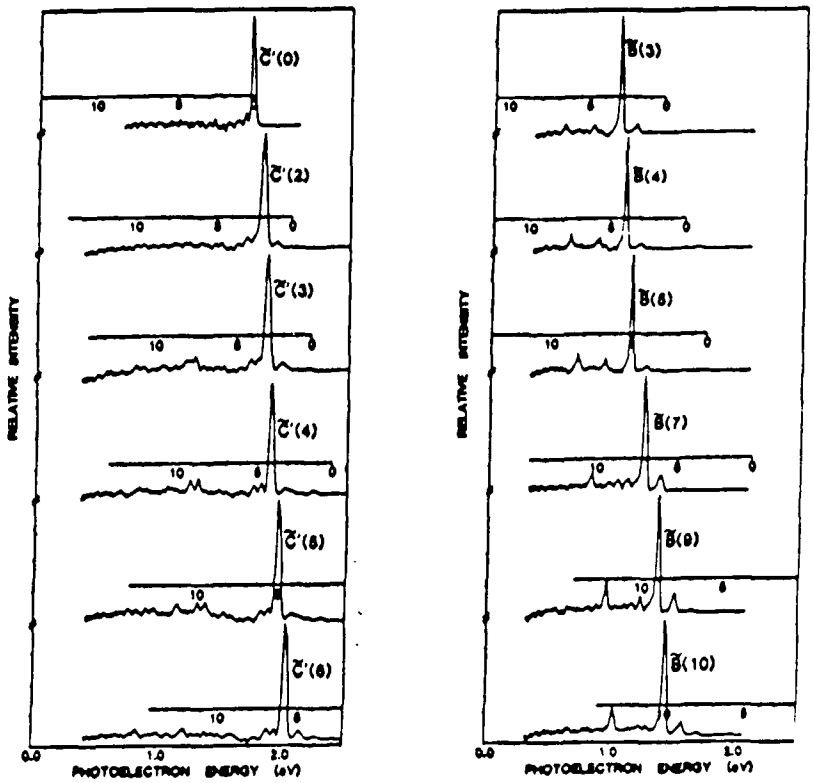

Figure 3. Photoelectron kinetic energy distributions for the $\tilde{B}$ and $\tilde{C}'$ states of ammonia.

be controlled over the range 0–50 eV by adjusting the potentials applied to the ion lenses. Forward scattered products and unreacted primary ions are mass analyzed by a quadrupole mass spectrometer equipped with a channel electron multiplier array. The signal is subsequently pulse counted or amplified and recorded by a computer. The computer is also used for scanning the primary ion energy and for tuning the mass control of the quadrupole. It is therefore possible to measure the yield of product ions as a function of both the reagent ion vibrational state and its kinetic energy.

(a) $NH_3^+(v_2) + CH_4$

The effects of vibrational excitation of the ammonia v_2 inversion mode on the reaction of $NH_3^+(\tilde{X}, v = 0\text{–}9)$ with methane have been measured[2] in a tandem quadrupole mass spectrometer over the center-of-mass colli-

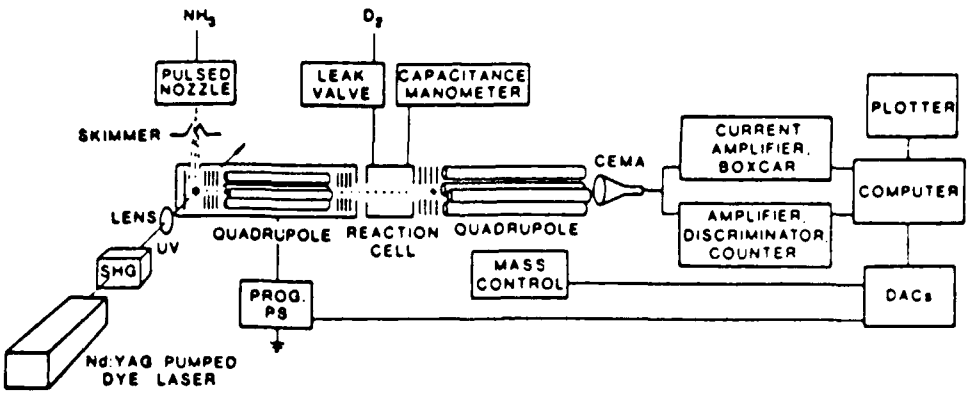

Figure 4. Schematic diagram of the tandem quadrupole mass spectrometer with laser multiphoton ionization source.

sion energy range 1.5 -10 eV. The hydrogen abstraction channel is enhanced by nearly a factor of two at nine quanta of vibrational energy relative to the $v = 0$ level of the ion. Added vibration in the ammonia ion umbrella-bending mode facilitates the transition to the NH_4^+ product ion geometry. Protonated methylamine is formed at lower kinetic energies by attack of the ion at the methane carbon center, but with increasing vibrational excitation of the ammonia ion, the protonated methylamine decomposes by 1,2-elimination of the molecular hydrogen and by C-N bond scission (see Fig. 5).

In summary, direct hydrogen atom abstraction is the dominant reaction pathway for the $NH_3^+(v) + CH_4$ system in the kinetic energy range studied. Vibrational excitation of the NH_3^+ umbrella-bending mode enhances the abstraction reaction by improving the dynamics of the transition into the NH_4^+ product channel. The CH_3-NH_3^+ condensation product appears at low kinetic energy and its formation is unaffected by the initial ion vibrational state. There is evidence for a small barrier associated with the displacement reaction to form this product ion, and the reaction mechanism may be

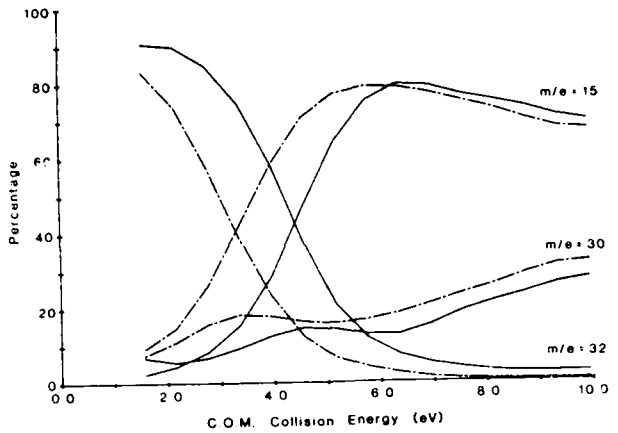

Figure 5. Vibrational energy dependence of the CH_3- NH_3^+ (m/e=32), $CH_2{=}NH_2^+$ (m/e=30), and CH_3^+ (m/e=15) ion signals as a percentage of the sum of the ion signals for these three ions. The solid line is for the reaction $NH_3^+(v = 8) + CH_4$. Because the collection efficiency varies with the ion, the important features are the relative changes of m/e=15, 30, and 32, not the absolute changes.

of the S_N2-type. At higher energies, the CH_3-NH_3^+ ion decomposes by 1,2-elimination of molecular hydrogen across the C-N bond and by C-N bond scission (see Fig. 6). The vibrational energy of the ammonia ion is randomized in the condensation product before decomposition and makes a significant energetic contribution to the internal energy of the complex. The appearance of the $CH_2 = NH_2^+$ product is consistent with previous reports[3] of a 2.6 eV energy barrier in the CH_3-NH_3^+ decomposition channel.

(b) $NH_3^+(v_2)+ND_3$ and $ND_3^+(v_2) + NH_3$

The role of vibrational excitation of the ν_2 umbrella-bonding mode of $ND_3^+(\tilde{X}, v{=}0$ to 10) and $NH_3^+(\tilde{X}, v{=}0$ to 9) on the reaction with NH_3 and ND_3 has been examined[4] over the 2–12 eV center of mass kinetic energy range. Isotopic substitution permits the investigation of charge transfer, proton/deuteron transfer, and neutral atom abstraction. The charge transfer channel is moderately enhanced by excitation of the ammonia ion ν_2

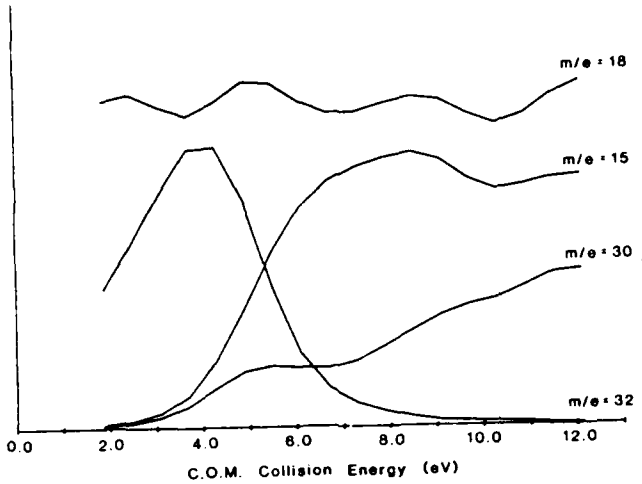

Figure 6. Kinetic energy dependence of the CH_3^+ (m/e = 15), NH_4^+ (m/e = 18), CH_2 =NH_2^+ (m/e = 30), and CH_3-NH_3^+ (m/e = 32) product ion signals for $NH_3^+(v = 0)$ + CH_4 (1 mtorr).

vibrational mode (Fig. 7). The proton/deuteron transfer channel is suppressed by vibrational excitation of the ion at low kinetic energies (Fig. 8). The hydrogen/deuterium atom abstraction channels show nearly a factor of six vibrational enhancement relative to $NH_3^+(v = 0)$ (Fig. 9). The ion vibrational and translational energy play inequivalent roles in the reactions, indicating that non-statistical factors are important in the transition from reactant to product channels. A simple dynamical model has been proposed to explain both the proton/deuteron transfer and the neutral atom abstraction reactions, it is based on the argument that vibrational motion along the particle transfer coordinate (Fig. 10A) promotes reaction while vibrational motion perpendicular to the transfer coordinate (Fig. 10B) hinders reaction.

In summary the proton/deuteron transfer channel and the neutral atom abstraction channel provide unique insight into the coupling of the ammonia ion vibrational motion into the reaction coordinate for each mechanism. The fact that the vibrational energy and translational energy of the ion af-

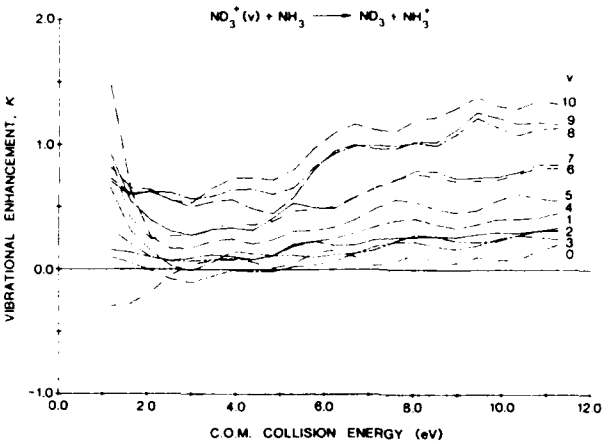

Figure 7. Vibrational dependence of the relative cross section of the charge transfer reaction between $ND_3^+(\nu_2)$ and NH_3 for $v = 0$–9. The reproducibility of the $v = 0$ curve indicates the magnitude of the error associated with the scatter in the data points and the normalization between the vibrational data sets.

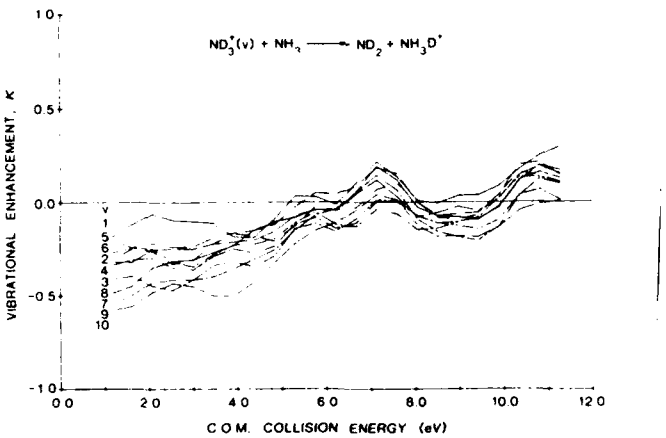

Figure 8. Vibrational dependence of the relative cross section of the deuteron transfer reaction between $ND_3^+(\nu_2)$ and the NH_3 for $v = 0$–10.

fect the relative reaction cross section to different extents indicates that these reactions are better described by a dynamical rather than a statistical model. Both dynamic and structural features of the transition state appear to play a role in determining which mechanism is operative and whether

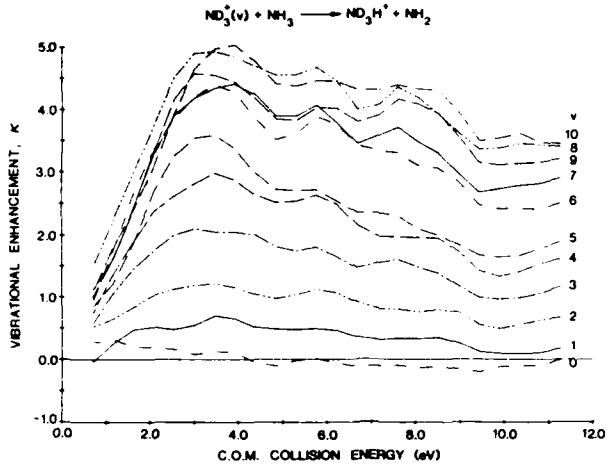

Figure 9. Vibrational dependence of the relative cross section of the hydrogen atom abstraction reaction between $ND_3^+(\nu_2)$ and NH_3 for $v = 0$–10.

A B

Figure 10.

it is suppressed or enhanced by vibration in the ion. In the case of photon transfer, motion of the the nuclei of the ion perpendicular to the direction of transfer ninders the formation of NH_4^+, while for hydrogen abstraction, the same motion perpendicular to the direction of hydrogen transfer favors formation of the NH_4^+ product ion.

(c) Vibrational Dependence of the $NH_3^+ + (v_2)$ + NH_3 Symmetric Charge Transfer Reaction

Vibrational overlap integrals have been calculated[5] for the transition between the neutral ground state and the ion state of NH_3 and ND_3 for the

ν_2 vibrational bending mode. Calculations were performed by numerically solving the Schrödinger equation. The vibrational overlap integrals were used to simulate the dependence of the cross section for the $NH_3^+(v_2) + NH_3(0) \rightarrow NH_3(v_2'') + NH_3^+(v_2')$ symmetric charge transfer reaction on the initial vibrational quantum state of the ion. The cross sections show a gradual increase with v_2, in agreement with experiment of Baer and Murray.[6]

Many charge transfer theories have been developed based on calculations using Franck-Condon factors for transition connecting the neutral and ion states. In this study, we have evaluated the vibrational overlap integrals for the ν_2 bending mode between the neutral ground state and ion ground state of the ammonia molecule and have calculated the v_2 dependence of the $NH_3^+(v_2) + NH_3(0) \rightarrow NH_3(v_2') + NH_3^+(v_2')$ symmetric charge transfer reaction cross section. The calculations have been carried out for $v_2 = 0$ up to $v_2 = 5$ and include both resonant and non-resonant charge transfer channels.

The theoretical approach used to calculated the state-to-state cross sections for symmetric charge transfer reactions is based on the work of Bates and Reid[7] and of Moran and coworkers,[8] who introduced the multistate impact parameter model. The model uses the time-dependent Schrödinger equation for the internal vibrational motion and classical trajectories for the relative translational motion. This treatment has been extended by DePristo.[9] The results of DePristo show excellent agreement with the exact quantal calculations of Becker[10] on the $O_2^+ + O_2$ symmetric charge transfer system.

For the $NH_3^+(v_2) + NH_3(0)$ reaction, the calculation was performed at the center-of-mass collision energy of 10 eV to allow direct comparison with the experimental results reported by Baer and Murray. Figure 11 shows the absolute value of the charge transfer (exchange) probability as a function

of impact parameter for the ammonia ion initially populated in the $v_2 = 0$ state. The resonant charge transfer channel is not a dominant channel and the reaction path is broadly distributed over the nonresonant channels. In the present model, the reaction pathways with large vibrational overlaps and small energy defects with respect to the initial channel make the largest contribution to the cross section. However, ammonia undergoes a large geometric change from the pyramidal neutral ground state to the planar ion state, causing the Franck-Condon factors $| <NH_3^+(v_2')|NH_3(0)> |^2$ to have a maximum value when $v_2' = 5$. Therefore, the resonant charge transfer channel cannot be a major channel because the product of the vibrational overlap integrals is very small compared to the nonresonant channels. The large contribution by off-diagonal Franck-Condon factors distinguishes the symmetric ammonia charge transfer system from systems such as $O_2^+ + O_2$, $N_2^+ + N_2$, and $CO^+ + CO$.

2. The octapole ion trap

The above studies using the tandem quadrupole mass spectrometer were limited to the collection of forward scattered products over a relatively narrow range of forward scattering angles. Additionally, the employment of a static lens system (collision cell region) after an rf device (first quadrupole of the tandem system) resulted in significant loss in reactant ion intensity because of the time-dependent trajectory of ions exiting an rf field. For the studies above, this prevented the determination of such factors as relative branching ratios and cross sections for the various reaction channels.

As a solution to this problem, we proposed replacing the static collision cell with an octapole ion-trap. When constructed, this would allow for efficient passage of ions from one rf region to the next and collection efficiencies approaching 100% for all ion products and scattered reactants, irrespective

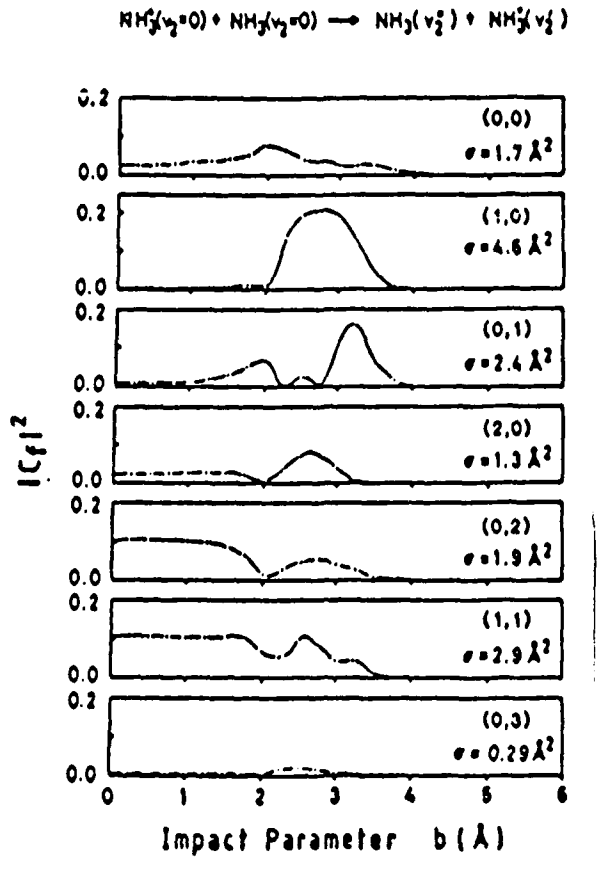

Figure 11. Plot of the transition probability of the exchange channel versus impact parameter for the reaction $NH_3^+(0) + NH_3(0) \rightarrow NH_3(v_2'') + NH_3(v_2')$ at a center-of-mass collision energy of 10 eV. The numbers in parentheses represent (v_2', v_2'').

of their final laboratory energy or direction. Our instrument is now completed and operational as shown schematically in Fig. 12. We review its features briefly.

A pulsed molecular beam is formed via a supersonic expansion from a steerable pulsed valve in a doubly differentially pumped chamber. The skimmed and collimated neutral beam enters an ionization chamber where ions are formed either by conventional electron impact or by REMPI from a tunable pulsed laser system. Ions are extracted out of the neutral beam and focused into the ion optic quadrupole/octapole/quadrupole system by a 90°

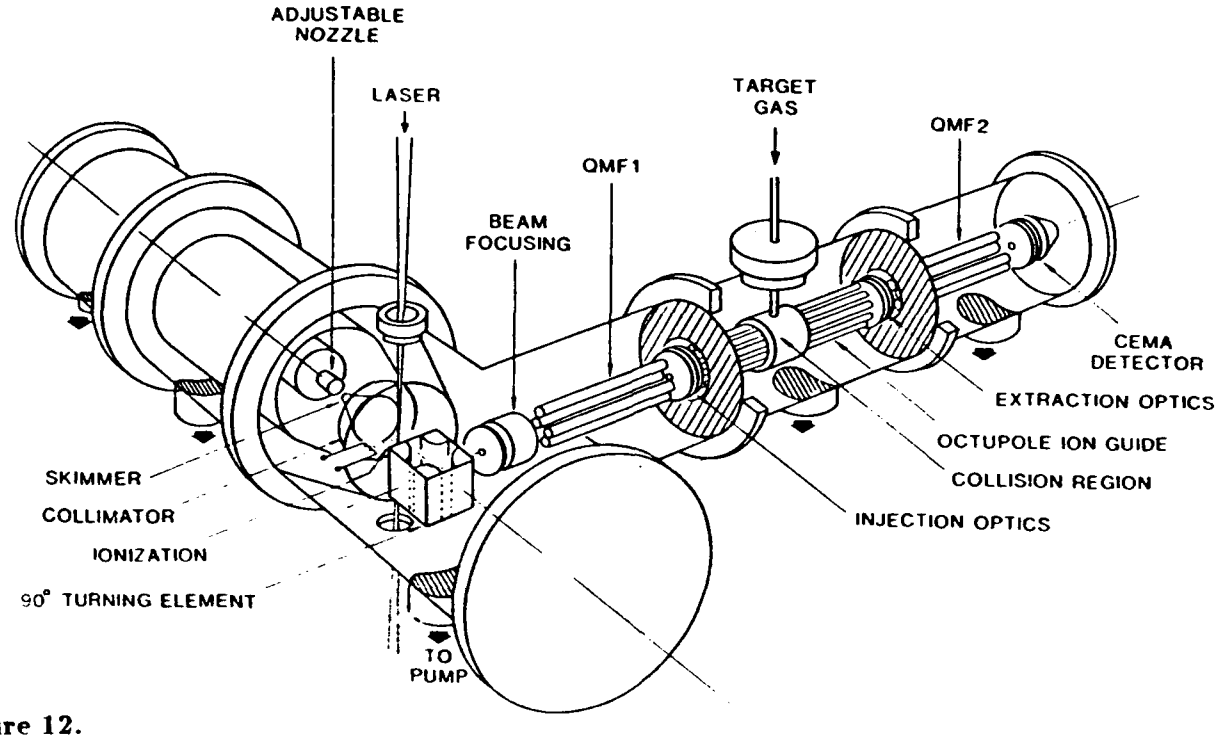

Figure 12.

quad turning element. The ions are focused into the first quadrupole, mass selected, and injected into the octapole ion trap with a known translational energy and energy spread. As the ions move slowly through the octapole trap they pass through a narrow collision cell containing the thermalized neutral collision gas. All ions, both unreacted elastically scattered reactant ions and product ions, are constrained by the radial field of the trap to only forward or backward laboratory motion. The ions are extracted from the octapole, accelerated, and injected into the second quadrupole for mass selection. The final mass-selected ion beam is measured with a multichannel plate chevron. Data are recorded simultaneously in two modes: using single ion counting with a fast MCA for repetitive time averaging (weak signal limit), and using a transient digitizer (strong signal limit).

In order to characterize the instrument fully and ensure that its limits

are clearly understood, we have chosen the well-characterized reaction[11]

$$\begin{aligned} Ar^+ + H_2 \rightarrow \quad & Ar + H + H^+ \\ \rightarrow \quad & Ar + H_2^+ \\ \rightarrow \quad & ArH^+ + H \end{aligned}$$

We are presently measuring these reactions and comparing them with results obtained using numerous other techniques. Once we feel comfortable with these results, we can press ahead with intended studies reviewed in the next section.

However, during the course of the past year we note that several significant and unexpected problems were encountered (and subsequently solved) in the construction of this device. These problems centered around the linking of three independent rf ion optic devices in a manner that guarantees minimal ion loss (and hence mass discrimination) at the rf device interface and without significant deterioration in the kinetic energy spread of the ions. Such properties are not apparent in similar devices currently being used by other groups. These problems were addressed through extensive use of computer modeling for both the static and rf ion optics, and we found it necessary to redesign several elements of the optic train in order to meet this requirement.

(Because of the usefulness of linking multiple rf devices, we wish to state the interfacing method here briefly. Ions exiting an rf device have a broad angular divergence that is time dependent on the rf voltage at the moment the ion leaves the local rf field. Subsequently, the resulting ion train is no longer compatible with any fixed static lens systems since each ion has a different trajectory. However, we found that by strongly accelerating the exiting ions through a very thin symmetric einsel lens, all the ions could

be brought through a single approximate focal point halfway between the two rf devices. As the ions are decelerated, they again plume in a wide divergence, each with its own time-dependent trajectory. We may now take advantage of the wide angular acceptance of the subsequent rf device. By keeping the distance between consecutive rf devices as short as possible, the expanding ion plume may be efficiently decelerated and captured in the next rf device without undue degradation in ion energy spread. The proper design of the interface lenses requires the use of rather sophisticated computer modeling programs[12] that have recently become available.)

Since the operation of the instrument is essentially in a pulsed mode, the data is recorded in a TOF manner, as noted above, providing a continuous and permanent record of the energy spread and spread symmetry of the measured ion. This technique is absolutely necessary to ensure that proper focusing is maintained and documented over the range of translational energy and ion mass selection required by the experiments.

One outcome of addressing these design problems is that we believe that absolute reaction cross sections may be measured with the instrument. In the absence of significant mass discrimination (or at least quantifiable mass discrimination) the use of simultaneous time-averaged single ion counting for weak product ion detection and analogue methods, calibrated in the low and medium signal range where ion counting and analogue signal overlap, allows us to quantify both reactant and product ion signal. We believe that this will allow us to measure for the first time absolute cross sections.

A second useful, though less certain, measure potential of the instrument is the extraction of scattering angle and energy distributions of the product ions from the TOF distributions. Because the temporal and hence energy distribution of both reactants and products is the method of data

measurement, and since the octapole potential within which the reactive scattering occurs is readily calculable, it appears that, in principle, low resolution energy and angle measure could be extracted from the TOF distributions. Such measurements may be limited to examples where the amplification factor[13] is at a maximum (light ion, heavy neutral products).

In summary, the operational instrument, shown in Figure 14, is more sophisticated than was originally intended. However, we believe that our experimental capabilities are greatly enhanced, including the ability to make absolute cross section measurements and possibly low resolution angle resolved product energy distributions in favorable product cases. We are presently conducting benchmark studies for the $Ar^+ + H_2$ system. Studies on the state-selected ammonia ion system will follow.

REFERENCES

[1] S. W. Allendorf, D. J. Leahy, D. C. Jacobs, and R. N. Zare, *J. Chem. Phys.* (accepted).

[2] W. E. Conaway, T. Ebata, and R. N. Zare, *J. Chem. Phys.* **87**, 3447 (1987).

[3] M. T. Bowers, W. J. Chesnavich, and W. T. Huntress, *Int. J. Mass Spectrom. Ion Physics* **12**, 357 (1973).

[4] W. E. Conaway, T. Ebata, and R. N. Zare, *J. Chem. Phys.* **87**, 3453 (1987).

[5] T. Ebata, W. E. Conaway, and R. N. Zare, *Int. J. Mass Spectrom. Ion Proc.* **80** 51 (1987).

[6] T. Baer and P. T. Murray, *J. Chem. Phys.* **75**, 4477 (1981).

[7] D. R. Bates and R. H. G. Reid, *Proc. R. Soc.* **A310**, 1 (1969).

[8] T. F. Moran, K. J. McCann, and M. R. Flannery, *J. Chem. Phys.* **63**, 3857 (1975).

[9] A. E. DePristo, *J. Chem. Phys.* **79**, 1741 (1983).

[10] C. H. Becker, *J. Chem. Phys.* **76**, 5928 (1982).

[11] See, for example, K. M. Ervin and P. B. Armentrout, *J. Chem. Phys.* **84**, 6738 (1986); *J. Chem. Phys.* **90**, 118 (1989).

[12] Program Simion V. 4.1, DOC #EGG-CS-7233, D. A. Dahl and J. E. Delmore, Idaho National Engineering Laboratory, EG&G Idaho, Inc., P. O. Box 1625, Idaho Falls, ID 83415.

[13] See, for example, R. G. Cooks, J. H. Beymon, R. M. Caprioli, and R. G. Lester, *Metastable Ions*, Elsevior, Amsterdam (1983).

PUBLICATIONS

Vibrational Dependence of the $NH_3^+(v_2)$ + NO and $NO^+(v)$ + NH_3 Charge Transfer Cross Sections, T. Ebata and R. N. Zare, *Chem. Phys. Lett.* **130**, 467 (1986).

BaI Product State Distribution from the Reaction Ba + CF_3I, M. A. Johnson, J. Allison, and R. N. Zare, *J. Chem. Phys.* **85**, 5723 (1986).

Vibrational Overlap Integrals between the Neutral and Ion States of NH_3 and ND_3: Application to the Vibrational Dependence of the $NH_3^+(v_2)$ + $NH_3(0)$ Symmetric Charge Transfer Reaction, T. Ebata, W. E. Conaway, and R. N. Zare, *Intl. J. Mass Spectrom. Ion Proc.* **80**, 51 (1987).

Vibrationally State-Selected Reactions of Ammonia Ions. II. $NH_3^+(v)$ + CH_4, W. E. Conaway, T. Ebata, and R. N. Zare, *J. Chem. Phys.* **87**, 3447 (1987).

Vibrationally State-Selected Reactions of Ammonia Ions. III. $NH_3^+(v)$ + ND_3 and $ND_3^+(v)$ + NH_3, W. E. Conaway, T. Ebata, and R. N. Zare, *J. Chem. Phys.* **87**, 3453 (1987).

High-Resolution Angle- and Energy-Resolved Photoelectron Spectroscopy of NO: Parial Wave Decomposition of the Ionization Continuum, S. W. Allendorf, D. J. Leahy, D. C. Jacobs, and R. N. Zare, *J. Chem. Phys.*, (in press).

PERSONNEL

Graduate Students

Sarah W. Allendorf, Ph.D. 03/13/89, "Angle- and Energy-Resolved Photoelectron Spectroscopy: A Probe of Photoionization Dynamics."

William E. Conaway, Ph.D. 02/18/87, "Vibrationally State-Selected Reactions of Ammonia Ions."

David J. Leahy

Jinchun Xie

Post-doctoral

Dr. Takayuki Ebata

Dr. Beat A. Keller

Dr. Nicholas J. Kirchner